Correlation versus mean-field contributions to excitons, multiexcitons, and charging energies in semiconductor quantum dots

J. Shumway, A. Franceschetti, and Alex Zunger
National Renewable Energy Laboratory, Golden, Colorado 80401
(Received 2 October 2000; published 30 March 2001)

Single-dot spectroscopy is now able to resolve the energies of excitons, multiexcitons, and charging of semiconductor quantum dots with $\lesssim 1$ meV resolution. We discuss the physical content of these energies and show how they can be calculated via quantum Monte Carlo (QMC) and configuration interaction (CI) methods. The spectroscopic energies have three pieces: (i) a ''perturbative part'' reflecting carrier-carrier direct and exchange Coulomb energies obtained from *fixed* single-particle orbitals, (ii) a ''self-consistency correction'' when the single particle orbitals are allowed to adjust to the presence of carrier-carrier interaction, and (iii) a ''correlation correction.'' We first apply the QMC and CI methods to a model single-particle Hamiltonian: a spherical dot with a finite barrier and *single-band* effective mass. This allows us to test the convergence of the CI and to establish the relative importance of the three terms (i)–(iii) above. Next, we apply the CI method to a realistic single-particle Hamiltonian for a CdSe dot, including via a pseudopotential description the atomistic features, *multiband coupling*, spin-orbit effects, and surface passivation. We include all bound states (up to 40 000 Slater determinants) in the CI expansion. Our study shows that (1) typical exciton transition energies, which are ~ 1 eV, can be calculated to better than 95% by perturbation theory, with only a ~ 2 meV correlation correction; (2) typical electron addition energies are ~ 40 meV, of which correlation contributes very little (~ 1 meV); (3) typical biexciton binding energies are positive and ~ 10 meV and almost entirely due to correlation energy, and exciton addition energies are ~ 30 meV with nearly all contribution due to correlation; (4) while QMC is currently limited to a single-band effective-mass Hamiltonian, CI may be used with much more realistic models, which capture the correct symmetries and electronic structure of the dots, leading to qualitatively different predictions from effective-mass models; and (5) CI gives excited state energies necessary to identify some of the peaks that appear in single-dot photoluminescence spectra.

DOI: 10.1103/PhysRevB.63.155316 PACS number(s): 73.21.La, 78.66.−w, 71.45.Gm, 85.35.Be

I. INTRODUCTION: THE PHYSICAL CONTENT OF EXCITON, MULTIEXCITON, AND CHARGING ENERGIES IN DOTS

Small semiconductor dots, such as semiconductor-embedded Stranski-Krastanow (SK) dots or ''free-standing'' colloidal dots, are engineered and studied for their optical and transport properties.[1–3] Measurements on these dots have centered around quantities such as excitons,[4–6] multiexcitons,[7–11] and charging energies.[12–16] Advanced experimental techniques, such as single-dot spectroscopy, are able to resolve such energies to $\lesssim 1$ meV resolution. This article discusses the physical content of such measured quantities in terms of the mean-field (direct and exchange) Coulomb energies, which are relatively simple to model, and correlation energies, which we calculate by two leading methods in the field—quantum Monte Carlo (QMC) and configuration-interaction (CI) methods.

Let us consider a quantum dot with M holes in the valence band and N electrons in the conduction band. The total energy of the dot is $E_{M,N}(\alpha)$, where α is a quantum number that identifies the state of the system. Only differences in energy are accessible to experiment. We focus on four physical quantities.

(a) Exciton energies. The *exciton transition energy* $E_X^{(ij)}$ is the difference in total energy of a dot having as a dominant configuration an electron in level e_0 and a hole in level h_0 and a dot in the ground state,

$$E_X = E_{1,1}(e_0^1, h_0^1) - E_{0,0}. \tag{1}$$

Typical excitonic transition energies in III-V or II-VI dots, measured experimentally[5,17] by photoluminescence (PL) or by absorption, are 1–3 eV. The *exciton binding energy* Δ_X is the difference between the total energy of a system consisting of two infinitely separated identical dots, one with a hole in h_0 and the other with an electron in e_0, and the total energy of a quantum dot with an exciton:

$$\Delta_X = E_{1,0} + E_{0,1} - E_{1,1} - E_{0,0}, \tag{2}$$

where $E_{1,0}$ stands for $E_{1,0}(h_0^1 e_0^0)$, $E_{0,1} = E_{0,1}(h_0^0 e_0^1)$, and $E_{1,1} = E_{1,1}(h_0^1 e_0^1)$. Typical exciton binding energies in III-V and II-VI dots are 10–200 meV.[5,17]

(*b*) *Biexciton energies*. The *biexciton binding energy* Δ_{XX} is the difference between twice the exciton energy (or the energy of a system of two infinitely separated dots, each with an electron-hole pair), and the biexciton energy:

$$\Delta_{XX} = 2E_{1,1} - E_{2,2} - E_{0,0}, \tag{3}$$

where E_{22} stands for $E_{22}(h_0^2 e_0^2)$. The biexciton binding energy is positive (''bound biexciton'') when the total energy of two excitons in the same dot is lower than the energy of the two excitons in two separate dots. A bound biexciton appears as a redshifting of the exciton luminescence energy when a second exciton is present. This was seen in single-dot spectroscopy e.g., for InAs/GaAs.[7,8,11,18] Biexciton binding energies in III-V dots are 1–6 meV.[18–23]

(*c*) *Multiexciton energies*. The *Nth exciton charging energy* W_N is the minimum energy needed to add to a dot having $N-1$ electron-hole pairs (excitons) in their ground state one additional exciton,

$$W_N = E_{N,N} - E_{N-1,N-1}. \tag{4}$$

Physically, W_N is the highest possible energy for a photon emitted in the transition from the lowest energy state of N excitons to a state with $N-1$ excitons. The difference between successive multiexciton charging energies is the *Nth exciton addition energy* $\Delta^{(X)}_{N,N+1}$,

$$\Delta^{(X)}_{N,N+1} = W_N - W_{N-1} = E_{N+1,N+1} + E_{N-1,N-1} - 2E_{N,N}. \tag{5}$$

(*d*) *Electron loading energies*. The *electron charging energy* $\mu^{(e)}_N$ is the chemical potential needed to add an electron to a dot already having $N-1$ electrons,

$$\mu^{(e)}_N = E_{0,N} - E_{0,N-1}, \tag{6}$$

whereas the *electron addition energy* is the difference between two successive chemical potentials,

$$\Delta^{(e)}_{N,N+1} = \mu^{(e)}_N - \mu^{(e)}_{N-1} = E_{0,N+1} + E_{0,N-1} - 2E_{0,N}. \tag{7}$$

Electron addition energies in colloidal dots[14] are $\sim$200 meV, whereas in SK dots[12,24] they are $\sim$20 meV.

The definitions given here in Eqs. (1)–(7) are operational, model independent. A central question in the field is how to approximate these quantities through models. This requires knowing how much of the energy involved in the processes described by Eqs. (1)–(7) is due to ''mean-field'' effects, which can be modeled relatively simply, and how much is due to interparticle correlation, which is more intricate to model. Figure 1 illustrates the steps required to model the electronic and optical properties of a quantum dot: (a) choosing a structure (including size, shape, composition, and strain), (b) solving a single-particle model, and (c) treating interactions among the electrons and holes. In this paper we are concerned with *general* trends in correlation in dots, so we focus mainly on the choice of single-particle model, Fig. 1(b), and treatment of interactions, Fig. 1(c).

As illustrated in Fig. 1(b), the calculations of the quantities of Eqs. (1)–(7) require one to assume an underlying single-particle model, which determines the single-particle states (conduction electrons and holes). The single-particle model is cast as a Schrödinger equation with an effective single-particle potential. This potential contains all structural information about the system: the size, shape, composition, surfaces, interfaces of the dot system. Various levels of renormalization exist for the quantum dot single-particle model. The simplest is an effective mass (''particle-in-a-box'') model, in which the electron and hole excitations come from single parabolic bands. Better approximations are the multiband $k \cdot p$, tight-binding, and pseudopotentials methods.

The single-particle models do not usually contain the Coulomb interactions between the single-particle excitations (i.e., electron-electron, electron-hole, and hole-hole excitations). Instead, these interactions must be added to the model, as shown in Fig. 1(c). We classify the treatment of interaction among the single-particle excitations in three levels: (i) *first-order perturbation theory (PT)*,[7,25–29] which includes direct and exchange Coulomb interactions, *J* and *K*, evaluated from *fixed* single-particle orbitals; (ii) *self-consistent mean-field (MF) theory*,[30] in which the direct and exchange Coulomb terms are solved self-consistently [the difference between (ii) and (i) is called the ''self-consistency correction'' ΔE^{SC}]; and (iii) *correlated methods, such as CI* (Refs. 7,25–29) *or QMC*,[31–41] which include all many-body effects of interactions. The difference between the exact energy (iii) and the mean-field energy (ii) is called the ''correlation correction'' ΔE^{corr}. Thus, the energy for a dot with *M* holes and *N* electrons can be separated into three terms,

$$E^{\mathrm{tot}}_{M,N} = E^{\mathrm{PT}}_{M,N} + \Delta E^{\mathrm{SC}}_{M,N} + \Delta E^{\mathrm{corr}}_{M,N} \tag{8}$$

which are the perturbation theory energy $E^{\mathrm{PT}}_{M,N}$, the self-consistent corrections $\Delta E^{\mathrm{SC}}_{M,N}$, and the correlation correction $\Delta E^{\mathrm{corr}}_{M,N}$.

Due to computational limitations, the methods available to calculate correlation are dependent on which single-particle model is chosen (level of renormalization). The computational cost for accurately calculating correlation energies increases rapidly with the number of electrons one needs to

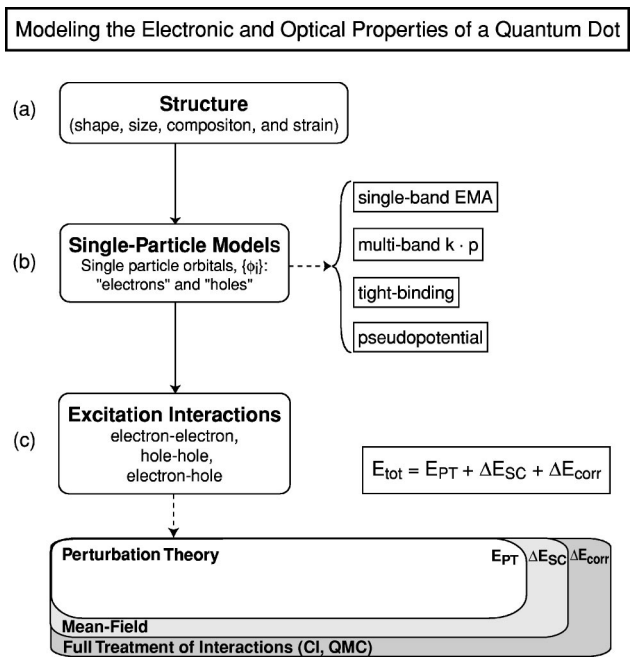

FIG. 1. The three steps to modeling a quantum dot. (a) The structure is modeled by choosing a size, shape, and composition profile, and determining the strain. (b) Single-particle properties of the electrons and holes are found by solving a Schrödinger equation for a chosen level of renormalization (EMA, $k \cdot p$, tight binding, or pseudopotential). (c) Interactions between excitations (electron-electron, electron-hole, hole-hole) are added to the single-particle model, using either perturbation theory E_{PT}, self-consistent mean-field theory, which adds the self-consistent contribution ΔE_{SC}, or full treatment (CI or QMC), which adds the correlation correction ΔE_{corr}.

TABLE I. Relationship between the choice of single-particle model for quantum dots and the availability of QMC and CI methods to calculate correlation energy [see Figs. 1(b) and 1(c)]. This information motivates our approach to studying correlation: first we test the convergence of CI against QMC calculations using a simple single-band EMA model, and then we present CI calculations on a realistic multiband pseudopotential quantum dot model to illustrate features missed by the simple model.

Level of renormalization	Model	CI[a]	QMC
All electron	exact Hamiltonian	no[b]	no
Valence only	multiband pseudopotential	yes	no[b]
	tight-binding	yes	no[b]
Active electron only	multiband $k\cdot p$	yes	no
	single-band EMA	yes	yes

[a]While CI may be applied to any model, it is often underconverged.
[b]Possible for very small clusters of fewer than 100 atoms ($R<10$ Å).

consider. The number of electrons depends on both the dot's size and the type of renormalization one uses for the Hamiltonian. As summarized in Table I, three levels of renormalization are pertinent.

(a) The all-electron approach, where the number of electrons per atom equals its atomic number. Thus, Si has 14 electrons per atom, and a 40 Å diameter spherical Si dot has $1600\times 14=22\,400$ electrons. This is outside the reach of QMC, CI, and density functional methods.

(b) The valence-only pseudopotential approach, where the ''core'' electrons are removed as dynamic variables and replaced by an (often nonlocal) ionic potential. Thus, Si has four electrons per atom, and a 40 Å diameter spherical Si dot has $1600\times 4=6400$ electrons. This is outside the reach of density functional methods, and too large for QMC calculations, which are currently limited to about 25 Si atoms (100 electrons).[42] Note that (in non-self-consistent calculations) the all-valence pseudopotential approach can be further simplified with no additional approximations by searching for eigensolutions in a fixed ''energy window,''[43–45] e.g., near the band edges. Thus, a 40 Å diameter Si dot would require calculating ~ 10 eigensolutions. This trick makes pseudopotential calculations of dots feasible,[26,30,46–48] and CI may be used to compute correlation energies from the single-particle solutions.[26–29] It would be interesting if such folding techniques could be applied to QMC.

(c) The ''active-electron-only'' effective-mass approximation (EMA) approach, where all of the ''indigenous'' core and valence electrons are eliminated (replaced by dielectric screening) and only *additional*, band-edge electrons and holes are considered. Thus a 40 Å diameter Si dot has zero electrons. One can study *added* electrons and holes. This renormalization represents a severe approximation with respect to levels (a) and (b) above. Both QMC and CI methods may be readily applied to single band EMA Hamiltonians. Some improvement can be made by using several bands to describe the additional electrons and holes using the $k\cdot p$ formalism,[49,50] but current QMC methods do not treat $k\cdot p$ Hamiltonians.

Most correlated calculations on quantum dots have used such a single-band effective mass model [level (c), above], where multiband and intervalley couplings are ignored. This particle-in-a-box description of the mean-field problem was recently[26,30,46–48] contrasted with the pseudopotential solution of the problem [(b) above] both for ''free-standing'' (colloidal) dots and for semiconductor-embedded SK dots. It was found that for ''free-standing'' dots such as InP,[46] and CdSe,[47] the effective-mass approach can lead to energy shifts of the order[46,47] ~ 500 meV; lead to reverse order of (s,p) levels;[46] miss more than half of the single-particle eigenvalues in a 0.5 eV energy range near the band edge;[47] underestimate the Coulomb integrals J_{ij} [Eq. (11)] by[30] $\sim 20\%$; and miss all the long-range part of the exchange integrals[26] K_{ij}. For pyramidal SK dots[48] the errors are somewhat smaller: shifts in the energy levels for electrons and holes are ~ 35 meV and ~ 110 meV, respectively; energy spacings from the EMA are about a factor of 2 too large; and the polarization ratio for dipole transitions along the two directions is 1 instead of 1.3. Such limitations in the EMA create a dilemma when modeling correlation as summarized in Table I. On one hand CI expansions may be applied to realistic single-particle models (e.g., pseudopotentials), but converge slowly with the number of configurations. On the other hand, QMC methods can give numerically exact answers including all correlation, but currently are limited to simple single-band effective-mass models. This situation prompts us to use the following strategy to study correlation effects: First, we consider a simplified ''particle-in-a-box'' single-band EMA model that can be treated via both QMC and CI. Our best CI calculations for the EMA model include all bound states, but neglect continuum states. Second, we consider a CdSe dot whose single-particle properties are described realistically by pseudopotentials, and the correlation is treated via CI only.

Our single-band EMA dot has been chosen to be representative of SK and colloidal dots. We summarize the properties of our model dot in Table II. We find the following results for the single-band model dot.

(i) Typical exciton transition energies for our model dots are ~ 1 eV, and typical exciton binding energies are ~ 50 meV. Of this, the MF gives $>95\%$ of the binding energy. Correlation is only ~ 2 meV, of which QMC provides an accurate solution. Although CI misses half the correlation energy, i.e., ~ 1 meV, it still captures $\sim 98\%$ of the total binding energy.

(ii) Typical biexciton transition energies for our dots are ~ 2 eV and typical biexciton binding energies are ~ 6 meV. The biexciton binding energy from mean-field theory is slightly negative (unbound biexcitons), so the positive biexciton binding is in fact due to ~ 6 meV of correlation energy. QMC captures all the correlation energy, whereas our CI captures only half (about 4 meV), so that the CI estimate of biexciton binding is only about 65% of the true value.

(iii) Typical electron charging energies for our dots are $\mu_1^{(e)}\approx 150$ meV, relative to the dot material conduction band

TABLE II. Measurable quantities for our single-band spherical model dot, with effective masses $m_e = 0.1$ and $m_h = 0.5$, dielectric constant $\epsilon = 12$, dot material band gap $E_{\rm gap} = 1$ eV, and band offsets $\Delta E_{\rm v} = 200$ eV and $\Delta E_{\rm c} = 400$ meV. For each quantity we give the magnitude (as calculated by QMC), the mean-field value, the correlation correction, and the percent of the energy recovered by CI expansion using all bound states. All energies are given in meV, and electron charging and total energies are measured relative to the dot material CBM.

Quantity	Magnitude	Mean field	Correlation	% CI
Exciton *total* energy $E_{1,1}(e_0^1,h_0^1)$	1136.3	1138.3	2.0	100.1
Biexciton *total* energy $E_{2,2}(e_0^2h_0^2)$	2266.5	2277.3	10.9	100.2
Total energy of two electrons $E_{0,2}(e_0^2)$	335.0	335.8	0.8	100.1
Exciton *transition* energy E_X [Eq. (1)]	1136.3	1138.3	2.0	100.1
Exciton *binding* energy Δ_X [Eq. (2)]	46.2	44.1	2.0	97.8
Biexciton *binding* energy Δ_{XX} [Eq. (3)]	6.2	-0.6	6.8	64.5
1st exciton *charging* energy W_1 [Eq. (4)]	1136.3	1138.3	2.0	100.1
2nd exciton *charging* energy W_2 [Eq. (4)]	1130.1	1139.0	8.9	100.2
1st exciton *addition* energy $\Delta_{1,2}^{(X)}$ [Eq. (5)]	-6.2	0.6	6.8	64.5
1st electron *charging* energy $\mu_1^{(e)}$ [Eq. (6)]	147.5	147.5	0.0	100.0
2nd electron *charging* energy $\mu_2^{(e)}$ [Eq. (6)]	187.5	188.3	0.8	100.1
1st electron *addition* energy $\Delta_{1,2}^{(e)}$ [Eq. (7)]	40.0	40.8	0.8	101.4

minimum (CBM), while addition energies are $\Delta_{1,2}^{(e)} \approx 40$ meV. Of this, correlation energy is very small (~ 1 meV), so mean-field or even perturbation theory describes dot charging and addition energies very well.

For our realistic CdSe dot we find that CI can be effectively combined with an accurate pseudopotential description of the single-particle problem, thus incorporating surface effects, hybridization, and multiband coupling. Furthermore, CI can calculate excited states easily, thus obtaining the many transitions seen experimentally, rather than only the ground-state–to–ground-state decay calculated by conventional QMC (note, however, that extensions of QMC to several excited states are possible[51,52]).

II. METHODS OF CALCULATION

A. Uncorrelated methods: perturbation theory and mean-field methods

The first-order perturbation energy $E_{M,N}^{PT}$ [Eq. (8)] can be written analytically as

$$E_{M,N}^{\rm PT} = E_{0,0} + \left(\sum_c \varepsilon_c - \sum_v \varepsilon_v \right) + \sum_{v<v'} (J_{v,v'} - K_{v,v'}) + \sum_{c<c'} (J_{c,c'} - K_{c,c'}) - \sum_{v,c} (J_{v,c} - K_{v,c}), \tag{9}$$

where ε_i are the single-particle energies, $J_{i,j}$ are the direct Coulomb energies, and $K_{i,j}$ are the exchange energies. The single-particle energies ε_i are often obtained from the solution of an effective single-particle Schrödinger equation,

$$\left\{ -\frac{1}{2}\nabla^2 + V_{\rm eff} \right\} \psi_i = \varepsilon_i \psi_i , \tag{10}$$

where $V_{\rm eff}$ is an effective potential. The Coulomb and exchange energies are given in terms of the single-particle wave functions ψ_i by

$$J_{i,j} = \int \frac{|\psi_i(\mathbf{r})|^2 |\psi_j(\mathbf{r}')|^2}{\epsilon(\mathbf{r},\mathbf{r}')|\mathbf{r}-\mathbf{r}'|} d\mathbf{r} d\mathbf{r}' ,$$

$$K_{i,j} = \int \frac{\psi_i^*(\mathbf{r}) \psi_j^*(\mathbf{r}) \psi_i(\mathbf{r}') \psi_j(\mathbf{r}')}{\epsilon(\mathbf{r},\mathbf{r}')|\mathbf{r}-\mathbf{r}'|} d\mathbf{r} d\mathbf{r}' , \tag{11}$$

where ϵ is the dielectric constant of the quantum dot.

The self-consistent contribution $E_{M,N}^{\rm SC}$, given by the first two terms on the right hand side of Eq. (8), arises from the self-consistent rearrangement of the single-particle wave function in response to the electrostatic field, Eq. (11), generated by the excitation of electrons and holes.

B. The correlated, many-particle methods

1. Quantum Monte Carlo method

The original QMC method[53] was based on the variational technique, a simple yet powerful theoretical tool. In a variational calculation, one proposes a parametrized trial wave function $\Psi_T^{\{\lambda\}}(R)$, where λ represents a set of variational parameters and R represents the coordinates of all the particles. The energy expectation value

$$E_T^{\{\lambda\}} = \frac{\int dR \Psi_T^{\{\lambda\}*}(R) H \Psi_T^{\{\lambda\}}(R)}{\int dR \Psi_T^{\{\lambda\}*}(R) \Psi_T^{\{\lambda\}}(R)} \tag{12}$$

may be minimized with respect to the variational parameters λ to give an estimate for the ground state energy and ground state wave function. This integral may be evaluated analyti-

cally, or Monte Carlo integration may be used. In this simplest formulation, QMC is formally equivalent to the variational techniques commonly applied to excitons in nanostructures.[54] Because the integral is over all electron and hole coordinates R, variational QMC calculations resemble classical simulations: a configuration of particle positions R undergoes a random walk through configuration space, using the rules of Metropolis Monte Carlo integration. The sequence of configurations, $R_i, R_{i+1}, \ldots$, samples the density $|\Psi_T(R)|^2$.

The real power of QMC is that it can go beyond the variational formalism and actually project the true ground state energy from an input variational trial function Ψ_T.[55] By weighting the configuration as it samples configuration space, the random walk can be identified with the imaginary time propagator $\exp(-H\tau)$. In this diffusion Monte Carlo algorithm,[55,56] the random walk in configuration space actually samples $\Psi_T^*\Phi_0$ where Φ_0 is the true ground state wave function. The energy expectation value along the walk $E_0 = \langle\Psi_T|H|\Phi_0\rangle/\langle\Psi_T|\Phi_0\rangle$ is then the true ground state energy of the many-body Hamiltonian. That is, even though the true ground state wave function Φ_0 is never explicitly calculated, its energy can be sampled from a random walk. In the remainder of the paper, the term QMC will refer to the diffusion Monte Carlo algorithm, unless explicitly noted otherwise.

Applications of QMC to quantum dots have used variational QMC (VMC),[31] diffusion QMC,[32–37] and a path-integral formulation, related to the diffusion algorithm and based on Feynman path integrals.[38–41] Harju *et al.*[31] have used both direct diagonalization and VMC to calculate the ground state energy of up to six electrons in a two-dimensional harmonically confined dot. Diffusion QMC within the EMA has been used (1) by Austin[32] to calculate the binding energy of excitons in a spherical dot as a function of dot radius, (2) by Bolton[33] to calculate the energy of up to four electrons in a two-dimensional harmonically confined dot in the presence of a magnetic field, (3) by Shumway *et al.*[34] to calculate total energies for electron addition to a pyramidal dot, (4) by Pederiva *et al.*[35] to calculate ground and excitation energies for up to 13 electrons in a three-dimensional harmonically confined dot and compare to results from Hartree-Fock and the local spin density approximation, and (5) by Luczak *et al.*[37] to study energies of up to 20 electrons confined to a two-dimensional harmonic potential. Lee *et al.*[36] have used QMC within the EMA to study a pair of electrons in a two-dimensional parabolic confining potential. Path-integral (PI) QMC has been used by Egger *et al.*[39] to studied crossover from Fermi liquid to Wigner molecule behavior using PIMC within the EMA on up to eight electrons in a two-dimensional harmonically confined dot, and by Harting *et al.*[57] to calculate the total energy of up to 12 electrons in a two-dimensional harmonically confined dot.

2. Configuration interaction

In the CI approach, the solutions of the many-body Hamiltonian are expanded in terms of Slater determinants $|\Phi\rangle$ obtained by removing M electrons from the valence band and adding N electrons to the conduction band:

$$|\Psi\rangle = \sum_{h_1,\ldots,h_M} \sum_{e_1,\ldots,e_N} A(h_1,\ldots,h_M,e_1,\ldots,e_N) \times |\Phi_{h_1,\ldots,h_M,e_1,\ldots,e_N}\rangle, \tag{13}$$

where

$$|\Phi_{h_1,\ldots,h_M,e_1,\ldots,e_N}\rangle = d_{h_1}^\dagger \cdots d_{h_M}^\dagger c_{e_1}^\dagger \cdots c_{e_N}^\dagger |\Phi_0\rangle. \tag{14}$$

Here $d_{h_1}^\dagger, \ldots, d_{h_M}^\dagger$ create *holes* in the valence band states $h_1, \ldots, h_M$, while $c_{e_1}^\dagger, \ldots, c_{e_N}^\dagger$ create *electrons* in the conduction band states $e_1, \ldots, e_N$. The Hamiltonian is then diagonalized in the basis of Slater determinants $|\Phi\rangle$. This approach gives access to not only the ground state of the system, but also excited states.

Full CI (FCI) includes all possible determinants from a given (finite) set of single-particle basis functions, i.e., N_h hole orbitals and N_e electron orbitals. In the limit of an infinite set of basis functions, $(N_h,N_e)\rightarrow(\infty,\infty)$, FCI provides the exact many-body solution, which is equivalent to the QMC results. However, most CI applications use a small and finite basis set to solve the Schrödinger problem. Thus, even including in the CI expansion all possible Slater determinants from a finite number of single-particle states (FCI) does not provide an exact solution, in contrast to QMC. For our calculations we also use only a small, finite basis set of bound states, denoted (N_h,N_e); therefore ground state total energies from FCI will be above the true ground state total energy. A useful truncated CI basis is singles and doubles configuration interaction (SDCI), which is the set of all determinants obtained by exciting at most two particles (electrons or holes) from the ground state (or reference) determinant. SDCI is equivalent to FCI for a single exciton (or two electrons), but is an approximation for two or more excitons (or three or more electrons).

The CI method has been used in the past to solve the the many-body Schrödinger equation in the EMA,[9,25,58–61] and also in the tight-binding approximation.[62] More recently, the CI approach has been used in the context of the empirical pseudopotential method for single excitons,[26] electron and hole addition energies,[27,28] and multiexcitons.[29]

III. APPLICATION OF QMC AND CI METHODS TO A SINGLE-BAND EFFECTIVE-MASS DOT WITH FINITE BARRIER

We first use a simplified single-band EMA model that can be treated by both QMC and CI. Our reference system is a spherical dot with radius $R=40$ Å, effective masses $m_e = 0.1$ and $m_h = 0.5$, dielectric constant $\epsilon = 12$, and barriers $\Delta E_e = 0.4$ eV and $\Delta E_h = 0.2$ eV. The energies of the optical and electronic properties of this dot are summarized in Table II. We varied the radius from 0 to 80 Å, while keeping the barriers fixed. This yields a range of bound electron and hole states. The energies of the lowest (i.e., band-edge) states e_0

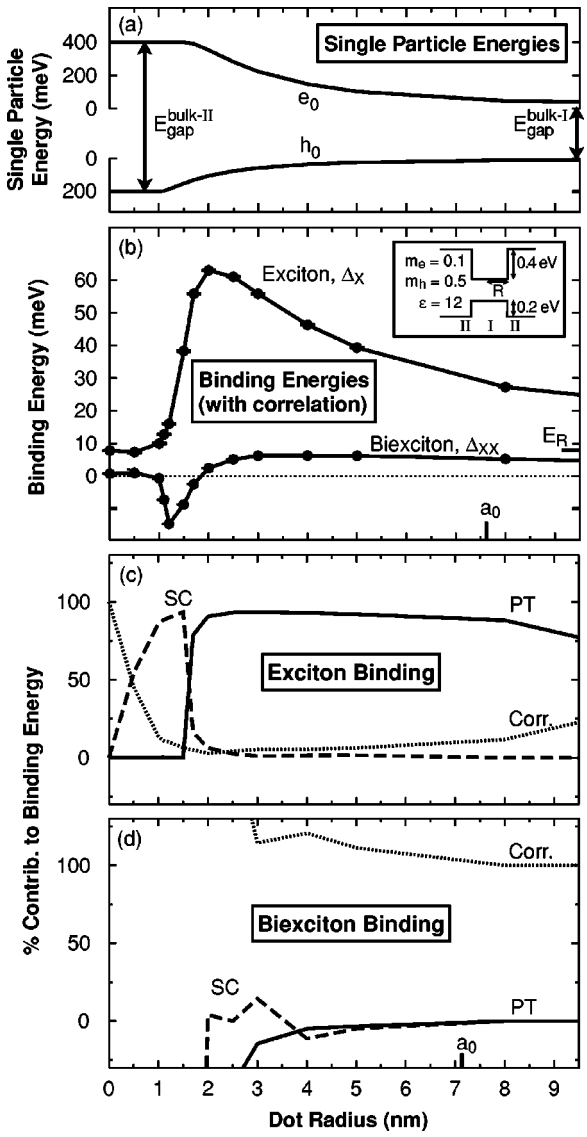

FIG. 2. Exciton and biexciton binding energy versus dot radius as calculated by QMC, for the dot geometry shown in the inset. Panel (a) shows the energies of the noninteracting electron and hole band-edge states. Panel (b) shows the the exciton binding energy Δ_X [Eq. (2)] and biexciton binding energy Δ_{XX} [Eq. (3)]. The bulk exciton Rydberg energy and Bohr radius are denoted $a_0=7.6$ nm and $E_R=7.9$ meV, respectively. Contributions to exciton and biexciton binding energy versus dot radius are shown in (c) and (d), respectively. Contributions are from first-order perturbation theory (PT), self-consistency correction (SC), and correlation (Corr.).

and h_0 as a function of dot radius R are shown in Fig. 2(a). When the radius R of the dot goes to infinity we have a three-dimensional (3D) bulk material called ''material I'' with $m_e=0.1$, $m_h=0.5$, and $\epsilon=12$. When the radius R of the dot goes to zero we have a 3D bulk material called ''material II'' with m_e, m_h, and ϵ identical to those of ''material I.'' The band offsets between the two materials are $\Delta E_h=0.2$ eV for the valence band and $\Delta E_e=0.4$ eV for the conduction band, so that the band gap of material II is $\Delta E_h+\Delta E_e=0.6$ eV larger than the band gap of material I. The bulk exciton in both materials is the same, and has a radius $a_0=76.2$ Å and a binding energy $E_R=7.873$ meV. Both bulk materials have a bound biexciton with the same binding energy $\Delta_{XX}^{\text{bulk}}=0.716\,\text{meV}=0.9E_R$ (calculated by QMC). In some calculations we have varied the barrier energy from $\Delta E_e=0.05$ eV to $\Delta E_e=1.6$ eV and $\Delta E_h=0.025$ eV to $\Delta E_h=0.8$ eV, while keeping the radius fixed at 40 Å. Our model system has thus been chosen to roughly capture some properties of small SK or colloidal dots, as summarized in Table II.

A. Total energies for occupation by an exciton, a biexciton, and two electrons

Figure 3 shows the total energy for (a) an exciton, $E_{1,1}(e_0^1,h_0^1)$; (b) a biexciton, $E_{2,2}(e_0^2,h_0^2)$; and (c) two electrons, $E_{2,0}(e_0^2,h_0^0)$. We have decomposed the total energies into the three parts listed in Eq. (8): first-order perturbation theory (E_{PT}), self-consistent mean-field theory ($E_{\text{PT}}+\Delta E_{\text{SC}}$), and the exact QMC result ($E_{\text{tot}}=E_{\text{PT}}+\Delta E_{\text{SC}}+\Delta E_{\text{corr}}$). We then plot the results of CI calculations as a function of the number of single-particle states (N_h,N_e) used to generate the CI basis set, taking either singles and doubles only (SDCI) or all possible determinants (FCI). The CI energies for one determinant are equivalent to the MF result, and the FCI values must reach the QMC result in the limit of an infinite basis. The total number of CI determinants for M holes and N electrons occupying N_h hole states and N_e electron states is $C_M^{2N_h}C_N^{2N_e}$, where $C_m^n=n!/[m!(n-m)!]$. The factors of 2 are due to the spin degeneracy of the single-particle states. Table III lists the actual number of determinants for each of the FCI and SDCI data points in Fig. 3. The first three lines of Table II give a summary of the role of correlation energy and CI convergence in the total energy of these three systems.

In each system, the total energy estimated by first-order perturbation theory is above the true ground state energy (as required by the variational principle). Self-consistency improves upon first-order perturbation theory, and correlation provides additional improvement. For excitons, the self-consistency decreases the energy by ~ 1 meV, and correlation gives another ~ 2 meV improvement. The total energy, however, is $E_{1,1}=1136$ meV. So, although our CI only recovers about half of the correlation energy, the total energy is overestimated by only about 0.1%. For the case of a biexciton, self-consistency also lowers the energy by ~ 2 meV, while correlation lowers the energy by another ~ 10 meV. In calculations on a strain induced dot, Braskén *et al.*[61] found that SDCI captured $\gtrsim 90\%$ of the correlation energy for multiexcitons, based on comparison to FCI for one to four excitons. In our biexciton calculations, we also find that SDCI recovers nearly as much correlation energy as FCI, but this represents only about half of the total correlation energy. Again, though, correlation represents a small part of the total energy of the biexciton, so CI (FCI and SDCI) overestimate the total energy by only $\sim 0.2\%$. For a dot containing two electrons, corrections beyond first-order perturbation theory are much smaller, ~ 1 meV. In fact, for the system calculated here, we find only a 0.35 meV decrease in the two-electron system with self-consistency, and correlation de-

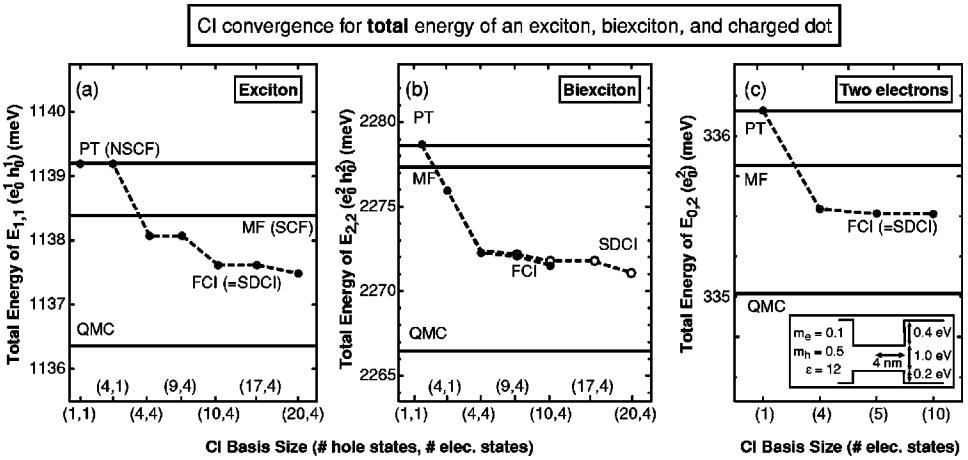

FIG. 3. CI convergence of the total energy for three cases: (a) an exciton, (b) a biexciton, and (c) two electrons. All energies are measured relative to the center of the dot gap. For our CI expansion, we have used single and double substitutions (SDCI) and also all possible determinants (FCI). Note that SDCI is equivalent to FCI for cases (a) and (c). SDCI gives a good approximation to FCI for case (b), and involves far fewer determinants (see Table III below). In all cases our CI expansion captures about half the correlation energy. The correlation energy (and hence CI error) is a very small fraction ($<1\%$) of the total energy in all three cases.

creases the total energy by about another 0.8 meV. Our CI expansion again captures about half this correlation energy, leading to a negligibly small overestimation of the total energy ($<0.1\%$).

TABLE III. Number of determinants used for each of the CI calculations shown in Figs. 3 and 4, using only single and double substitutions (SDCI), or all possible Slater determinants (FCI). Note that SDCI is equivalent to FCI for the case of an exciton or two electrons. For FCI the number of CI determinants for M holes and N electrons occupying N_h hole states and N_e electron states is $C_M^{2N_h} C_N^{2N_e}$.

		Number of determinants	
System	(N_h, N_e)	SDCI	FCI
Exciton (h^1e^1)	(1,1)	4	4
	(4,1)	16	16
	(4,4)	64	64
	(9,4)	144	144
	(10,4)	160	160
	(17,4)	262	262
	(20,4)	320	320
Biexciton (h^2e^2)	(1,1)	1	1
	(4,1)	28	28
	(4,4)	199	784
	(9,4)	564	4284
	(10,4)	649	5320
	(17,4)	1356	15708
	(20,4)	1719	21840
Two Electrons(h^0e^2)	(0,1)	4	4
	(0,4)	28	28
	(0,5)	153	153
	(0,10)	190	190

B. Exciton and biexciton transition and binding energies

Measured quantities such as the exciton and biexciton binding energies represent *differences* between total energies. Even if the mean-field contributions dominate total energies, the differences of total energies may have significant contributions from correlation. Lines 4–6 of Table II summarize the roles of correlation and CI convergence for the exciton transition energy E_X [Eq. (1)]; the exciton binding energy Δ_X [Eq. (2)]; and the biexciton binding energy Δ_{XX} [Eq. (3)]. Correlation is only a small part (2 meV) of the exciton transition energy $E_X = 1136.3$ meV. So, even though our underconverged CI fails to capture all the correlation energy, E_X is overestimated only by 0.1%. The same 2 meV of correlation energy is a much larger component of the exciton binding energy $\Delta_X = 46.2$ meV, so errors due to underconvergence of CI are more significant, and CI underestimates Δ_X by more than 2%. The biexciton binding energy $\Delta_{XX} = 6.2$ meV is due entirely to 6.8 meV of correlation energy, so CI underconvergence is much more serious. Our CI calculation of biexciton binding is only 65% of the exact QMC result.

In Fig. 4 we show the results of first-order perturbation theory (E_{PT}), self-consistent mean-field theory ($E_{\mathrm{PT}} + \Delta E_{\mathrm{SC}}$), the exact QMC result ($E_{\mathrm{tot}} = E_{\mathrm{PT}} + \Delta E_{\mathrm{SC}} + \Delta E_{\mathrm{corr}}$), and CI convergence vs basis size for (a) the exciton transition energy and (b) the biexciton binding energy. For the exciton transition energy, Fig. 4(a), increasing the CI basis does improve the calculated energy, but it is only a difference of ~ 2 meV out of a much larger exciton transition energy of 1.136 eV. On the other hand, the CI correction is essential to even approximate the biexciton binding energy, shown in Fig. 4(b). Note that the improvement of the biexciton binding with CI basis size is not monotonic. This is because the biexciton binding is a difference of one- and two-exciton energies. As the basis is increased, the relative improvement in the one- and two-exciton total energies var-

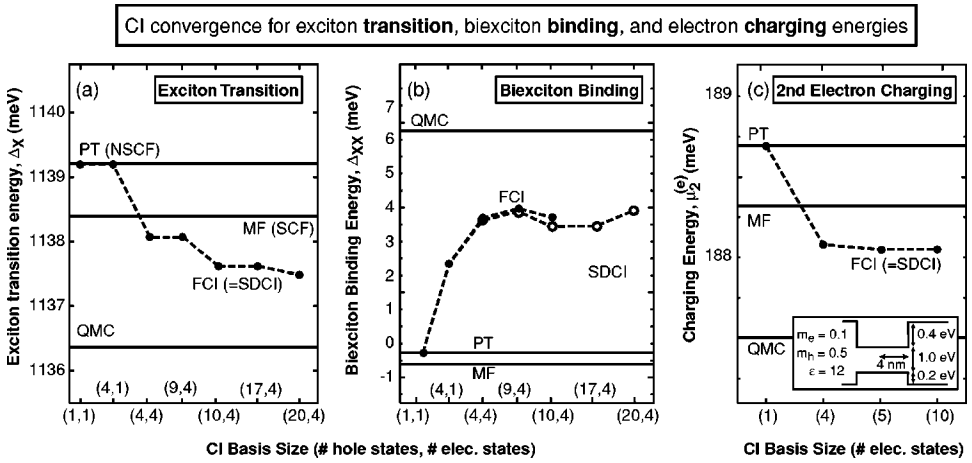

FIG. 4. CI convergence of (a) exciton transition energy E_X [Eq. (1)]; (b) biexciton binding energy Δ_{XX} [Eq. (3)]; and (c) second electron addition energy $\mu_2^{(e)}$ [Eq. (6)]. For our CI expansion, we have used single and double substitutions (SDCI) and also all possible determinants (FCI). Note that SDCI is equivalent to FCI for cases (a) and (c). SDCI gives a good approximation to FCI for case (b), and involves far fewer determinants (see Table III). In all cases our CI expansion captures about half of the correlation energy. The correlation energy (and hence CI error) is a significant fraction of the the total energy only for case (b), biexciton binding.

ies; thus the calculated biexciton binding energy can actually *decrease* when the CI basis is improved. We also show the results of SDCI in Fig. 4(b).

1. Dependence on dot size

We have varied the dot radius from $R=0$ to $R=80$ Å, all in the strongly confined regime, $R \lesssim a_0 = 76.2$ Å. Figure 2(b) shows the exciton and biexciton binding energies as calculated by QMC. Figures 2(c) and 2(d) decompose the contributions to the exciton and biexciton binding into (1) first-order perturbation theory, (2) self-consistency corrections, and (3) correlation corrections, as in Eq. (8).

The small R limit is the energy of a bulk-II material, and all excitonic binding energy is from correlation. As the radius of the dot increases, the bulk-II exciton binds to the dot, the exciton binding energy is enhanced, and most of the binding energy comes from perturbation theory. The maximum in the binding energy occurs when the electron and hole are both individually bound to the dot, but the radius is small, so that the direct Coulomb interaction (from first-order perturbation theory) is the strongest. The exciton binding energy exhibits a clear peak at around $R \approx 20$ Å, in similarity with previous calculations by Austin.[32] As the dot becomes larger, the direct Coulomb interaction from perturbation theory decreases, causing a decrease in the exciton binding energy. Finally, as the dot becomes comparable in size to the bulk-I exciton radius, correlation begins to make significant contributions to exciton binding. In the limit $R \gg a_0$ (not shown), the binding energy becomes that of a bulk-I exciton.

The biexciton binding energy is greatly enhanced in a quantum dot, except for the case of a very small dot with only a single weakly bound exciton. We find that the biexciton binding energy is remarkably insensitive to dot radius, having a value Δ_{XX} between 5.1 meV and 6.2 meV ($0.7E_R$ to $0.9E_R$) for dots with radii R between 2 nm and 8 nm ($0.3a_0$ and $1.1a_0$). This is in contrast to the exciton binding energy Δ_X, which exhibits a clear peak at small dot radius. The size range $10 \lesssim R \lesssim 18$ Å has a negative biexciton binding. Physically, these are small dots that can weakly bind two excitons, but with a higher total energy than if the two excitons are separated on two noninteracting, identical dots. We see from Fig. 2(d) that the biexciton binding energy is almost entirely due to correlation, as noted before.

2. Dependence on barrier height

To study the effect of finite confining barriers on exciton and biexciton binding energies, we have varied the dot barriers from zero to infinity. In all calculations we have kept $\Delta E_e / \Delta E_h = 2$ and used a radius of 40 Å. In Fig. 5(b) we plot the binding energies of excitons and biexcitons calculated with QMC as a function of barrier height. The 40 Å dot is able to bind an electron once $\Delta E_e \gtrsim 30$ meV, and binds a hole once $\Delta E_h \gtrsim 5$ meV. Unlike the behavior seen on varying the dot radius, increasing the confining potential leads to a monotonic increase in exciton and biexciton binding energies. For zero barrier potential, the exciton has the bulk-I exciton binding energy $\Delta_X = E_R^{(I)} = 7.9$ meV. As the barrier potential is increased enough to bind both electrons and holes, the exciton binding increases rapidly. The binding energy reaches a maximum of $\Delta_X = 55\,\text{meV} = 7E_R$ for infinite barriers. Similarly, the biexciton binding energy starts from the bulk biexciton binding energy $\Delta_{XX} = 0.7\,\text{meV} = 0.1E_R$ and increases to a maximum of $\Delta_{XX} = 7.2\,\text{meV} = 0.9E_R$ for infinite barriers. Figures 5(c) and 5(d) show the contributions of perturbation theory, self-consistency correction, and correlation to the exciton and biexciton binding energies. Except for very weakly confined dots, the exciton is very well described by first-order perturbation theory. For weak confinement, the electron is unable to bind, but self-consistent interaction with the hole is able to bind the electron, so that the exciton binding energy is almost entirely due to self-consistency. For the weakest confinement, neither the electron nor the hole is bound, and the excitonic binding is entirely due to correlation. Again, biexciton binding is due entirely to correlation.

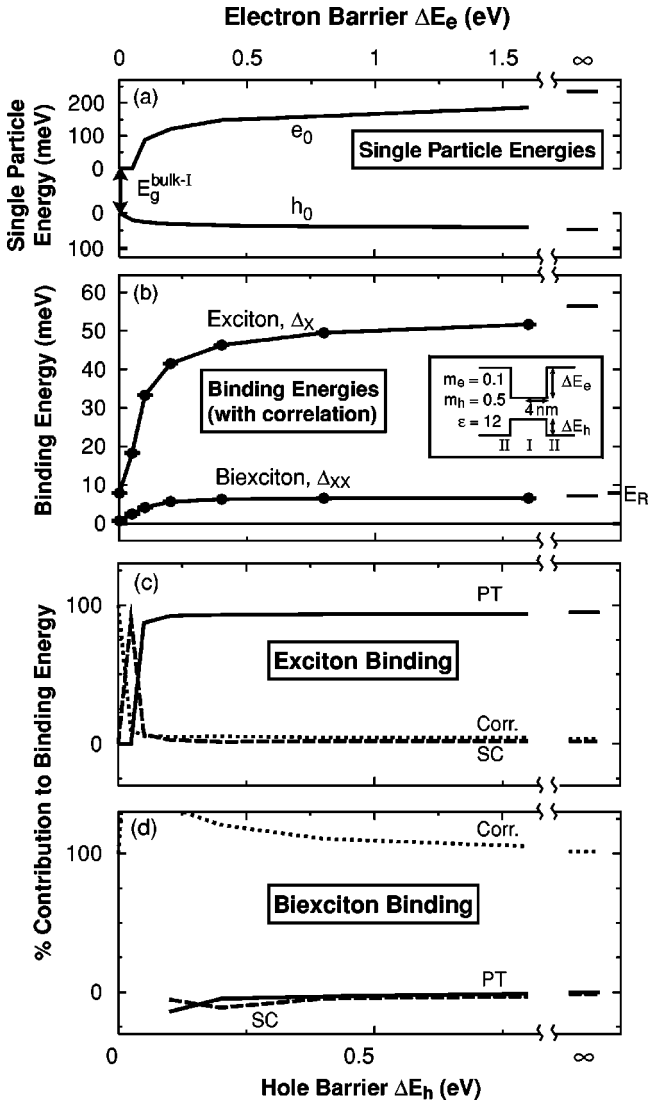

FIG. 5. Exciton and biexciton binding energies (including correlation) as calculated by QMC as a function of barrier energy, with the constraint $\Delta E_e/\Delta E_h=2$, for the dot geometry shown in the inset. Panel (a) shows the single-particle energies of the noninteracting electron and hole band-edge states. Panel (b) shows the the exciton binding energy Δ_X [Eq. (2)] and biexciton binding energy Δ_{XX} [Eq. (3)]. The bulk exciton Rydberg energy is denoted $E_R=7.9$ meV. Contributions to exciton and biexciton binding energies versus barrier energy are shown in (c) and (d), respectively. Contributions are from first-order perturbation theory (PT), self-consistency correction (SC), and correlation (Corr.).

C. Multiexciton energies

Figure 6 shows mean-field and exact (QMC) results for the multiexciton charging energies W_N [Eq. (4)], and the multiexciton addition energies $\Delta^{(X)}_{N,N+1}$ [Eq. (5)]. The most prominent feature is the jump in the charging energy for W_3, which also appears as a peak in the addition energy $\Delta^{(X)}_{2,3}$. This ''shell effect'' arises because only the first two excitons can occupy the lowest energy e_0 and h_0 states. Starting with the third exciton, Pauli exclusion requires the addition excitons to start filling the next energy shell, e_1h_1 through e_3h_3.

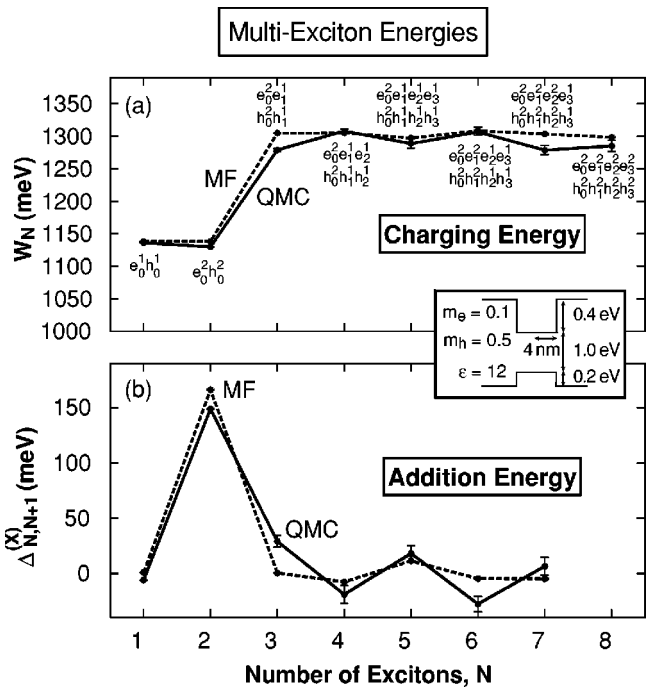

FIG. 6. (a) Exciton charging [Eq. (4)] and (b) addition energies [Eq. (5)], for the dot shown in the inset. Because excitons are neutral, it is energetically favorable for a dot to hold many excitons.

This is a feature of the single-particle model, and does not require any treatment of correlation. Correlation is necessary to describe the decrease in charging energy for the second exciton, $W_2<W_1$, or equivalently the negative value of the first exciton addition energy $\Delta^{(X)}_{1,2}=-6.2$ meV. This is the positive biexciton binding energy $\Delta_{XX}=6.2$ meV, discussed earlier. As shown in lines 7–9 of Table II, the correlation contribution for the second charging energy W_2 is 8.9 meV, considerably larger than the 2.0 meV for W_1. Our CI captures only about half the correlation energy, so it slightly overestimates the exciton charging energies, and considerably underestimates the negative value of $\Delta^{(X)}_{1,2}$.

D. Electron loading energies

Figure 7 shows mean-field and exact (QMC) results for electron charging energies μ_N [Eq. (6)], and the electron addition energies $\Delta^{(e)}_{N,N+1}$ [Eq. (7)]. Because electrons are charged, Coulomb repulsion quickly limits the number of electrons that can be loaded into the dot. For our model, shown in the inset to Fig. 7, it is only energetically favorable to add four electrons; beyond this, electrons would rather escape into the barrier material conduction band, shown as a dashed horizontal line in Fig. 7(a). There is a peak in the electron addition energy $\Delta^{e}_{2,3}$ in Fig. 7(b). This is due the filling of the e_0 state by a spin-up and spin-down electron (another ''shell effect''). Both QMC and MF capture this single-particle effect. As shown in Fig. 4(c), our CI expansion recovers about half the correlation energy for two electrons. However, the correlation energy in a two-electron dot is only about 1 meV, so CI errors are a negligible 0.5 meV.

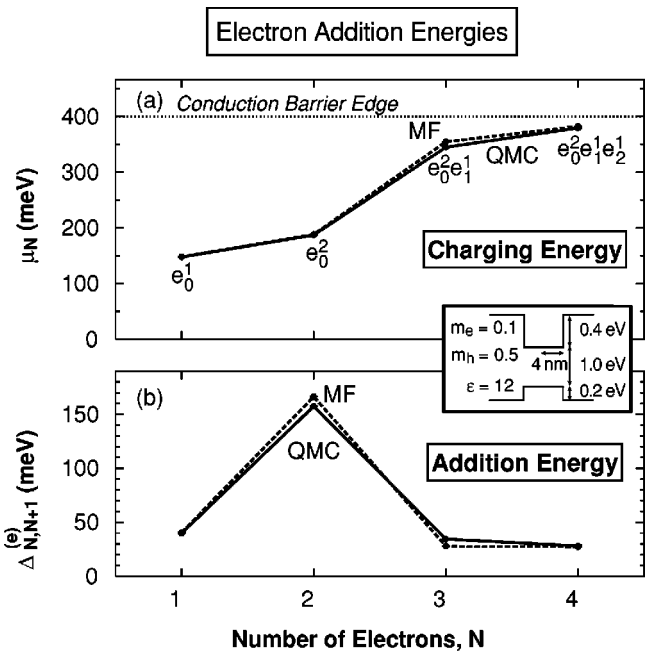

FIG. 7. (a) Electron charging energies [Eq. (6)] and (b) addition energies [Eq. (7)], for the dot shown in the inset. This dot can only hold up to four electrons, due to Coulomb repulsion. The conduction band minimum energy of the barrier material, $\Delta E_e = 400$ meV, is shown in panel (a).

The small value of correlation and the good agreement of our CI calculations for dot charging are summarized in the last three lines of Table II.

IV. APPLICATION OF CI TO A MULTIBAND DOT DESCRIBED VIA PLANE-WAVE PSEUDOPOTENTIALS

QMC calculations are currently limited to either small systems containing up to a few hundreds of electrons,[42,63,64] or highly simplified model Hamiltonians (such as the EMA). A more accurate description of the electronic structure (Fig. 1) of semiconductor quantum dots can be obtained using the pseudopotential approach.[48] Unfortunately, QMC methods are presently unable to deal with the large number of electrons of a typical quantum dot, and CI is the only viable approach to treat correlation effects in large quantum dots described by atomistic pseudopotentials. In addition, the diagonalization of the CI Hamiltonian gives access to the excited states (unavailable in ground state QMC calculations) as well as the ground state of the electronic system, thus enabling the calculation of the optical spectrum of quantum dots.

In order to illustrate the capabilities of the CI approach combined with a pseudopotential description of the electronic structure, we consider a nearly spherical CdSe quantum dot having the wurtzite lattice structure and a diameter of 38.5 Å. The surface dangling bonds are fully passivated using ligandlike atoms.[47] This quantum dot is representative of CdSe nanocrystals grown by colloidal chemistry methods.

We consider here only low energy excitations of the electronic system, which are obtained by promoting electrons from states near the top of the valence band to states near the bottom of the conduction band. The band-edge solutions of Eq. (10) can be efficiently obtained using the folded spectrum method,[43–45] which allows one to calculate *selected* eigenstates of the Schrödinger equation with a computational cost that scales only linearly with the size of the system. In this approach, Eq. (10) is replaced by the folded-spectrum equation

$$[-\nabla^2 + V_{ps}(\mathbf{r}) + \hat{V}_{NL} - \varepsilon_{ref}]^2 \psi_i(\mathbf{r},\sigma) = (\varepsilon_i^0 - \varepsilon_{ref})^2 \psi_i(\mathbf{r},\sigma), \tag{15}$$

where ε_{ref} is an *arbitrary* reference energy. The lowest energy eigenstate of Eq. (15) coincides with the solution of the Schrödinger equation [Eq. (10)] whose energy is closest to the reference energy ε_{ref}. Therefore, by choosing the reference energy in the band-gap, the band edge states can be obtained by minimizing the functional $A[\psi] = \langle \psi | (\hat{H} - \varepsilon_{ref})^2 | \psi \rangle$.

The solution of Eq. (15) is performed by expanding the wave functions $\psi_i(\mathbf{r},\sigma)$ in a plane-wave basis set. For this purpose, the total pseudopotential $V_{ps}(\mathbf{r})$ is defined in a periodically repeated supercell Ω containing the quantum dot and a portion of the surrounding material. The supercell Ω is sufficiently large to ensure that the solutions of Eq. (15) are converged within 1 meV. The single-particle wave functions can then be expanded as $\psi_i(\mathbf{r},\sigma) = \Sigma_{\mathbf{G}} c_i(\mathbf{G},\sigma) \exp(i\mathbf{G}\cdot\mathbf{r})$, where the sum runs over the reciprocal lattice vectors $\mathbf{G}$ of the supercell Ω. The energy cutoff of the plane-wave expansion is the same used to fit the bulk electronic structure, to ensure that the band structure consistently approaches the bulk limit. The minimization of the functional $A[\psi]$ is carried out in the plane-wave basis set using a preconditioned conjugate-gradient algorithm.

In the next step we construct a set of Slater determinants $|\Phi_{h_1,\ldots,h_N,e_1,\ldots,e_N}\rangle$ [see Eq. (14)] obtained by creating N holes in the valence band and N electrons in the conduction band, and diagonalize the CI Hamiltonian in this basis set. Using the CI approach, we have calculated the multiexciton spectrum of a CdSe dot. We consider here up to three excitons and we use a CI basis set of 480 configurations for the single exciton, 43 890 configurations for the biexciton, and 20 384 configurations for the triexciton. All the relevant interactions (including electron-hole exchange) are included in the CI calculations. We assume that when an N-exciton is created in the quantum dot it relaxes nonradiatively to the ground state before decaying radiatively into an $(N-1)$-exciton.

The calculated multiplet levels are shown in Fig. 8 and the emission spectrum is shown in Fig. 9. The three panels of Fig. 9 correspond to the recombination of (a) a triexciton into a biexciton $(3 \rightarrow 2)$, (b) a biexciton into a single exciton $(2 \rightarrow 1)$, and (c) a single exciton into the ground state $(1 \rightarrow 0)$, respectively. We assume that the low energy states of the N-exciton are thermally populated $(kT = 5$ meV) before recombination. We see the following from Fig. 9.

(i) The single-exciton recombination spectrum, Fig. 9(a), shows a single peak (A_1) centered at 2.154 eV. It is well known[65] that in CdSe nanocrystals the electron-hole ex-

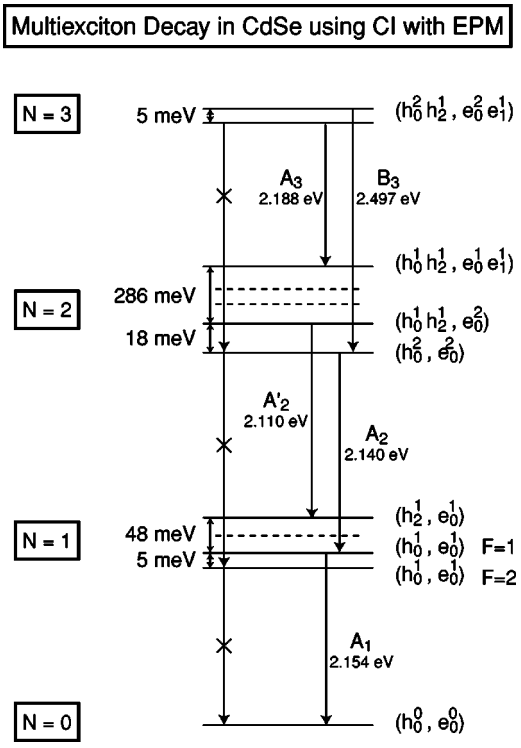

FIG. 8. Schematic illustration of the leading contributions to peaks $(A_3, B_3, A_2', A_2, A_1)$ appearing in Fig. 9. Solid horizontal lines are energies of $N=0$ to $N=3$ excitons, with dashed lines indicating one or more states that do not contribute to the major peaks in Fig. 9.

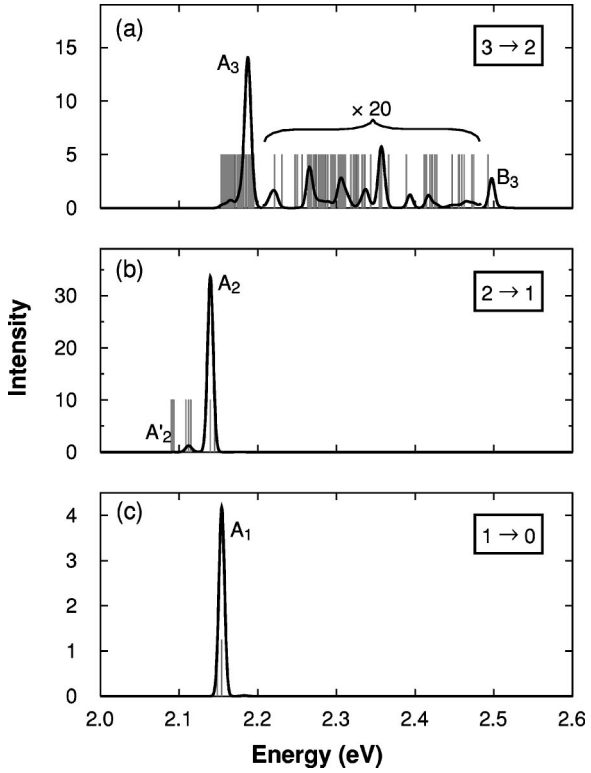

FIG. 9. Exciton transition energies for a CdSe dot for (a) decay from three to two excitons, (b) decay from two to one excitons and (c) decay of a single exciton. The intensity scale is different in each of the three panels, and weak transitions between peaks A_3 and B_3 in (a) have been magnified $\times 20$. Gray vertical lines indicate all calculated transition energies, and solid black lines in the Gaussian broadened transitions weighted by calculated dipole transition strengths.

change interaction splits the lowest energy excitonic state (h_0^1, e_0^1) into two doublets, having total angular momentum $F=2$ and $F=1$, respectively (see Fig. 8). The lower energy doublet $(F=2)$ is optically forbidden, while the higher energy doublet $(F=1)$ is optically allowed. We find an energy separation of ~ 5 meV between the two doublets. The emission peak A_1 observed in Fig. 9 comes from the recombination of the higher energy doublet, which is thermally populated. This explains the relatively weak intensity of the single-exciton peak.

(ii) The biexciton recombination spectrum, Fig. 9(b), shows a strong peak (A_2) centered at 2.140 eV. This peak originates from the recombination of a biexciton in the ground state (h_0^2, e_0^2) into a single exciton in the $F=1$ state. The weak shoulder to the red of the main peak (A_2') is due to the recombination of a thermally occupied higher energy biexciton state in the configuration $(h_0^1 h_2^1, e_0^2)$. Note that several transitions from the biexciton ground state to single-exciton excited states are in principle possible, but have very weak oscillator strength. These transitions would occur to the *red* of the fundamental transition. The calculated biexciton binding energy is $2E_X - E_{XX} \sim 4$ meV. This value is probably underestimated due to the underconvergence of the CI expansion. Interestingly, the ''apparent'' biexciton binding energy, i.e., the redshift of the main biexciton peak A_2 with respect to the single-exciton peak A_1, is ~ 14 meV (not 4 meV). The reason is that the biexciton recombination takes the quantum dot into the $F=1$ excited state, rather than the $F=2$ ground state (see Fig. 8). Thus we have

$$E(A_1) - E(A_2) = (E_X^{F=1} - E_{0,0}) - (E_{XX} - E_X^{F=1})$$
$$= \Delta_{XX} + 2(E_X^{F=1} - E_X^{F=2})$$
$$= 4 + 2 \times 5 \text{ meV} = 14 \text{ meV}.$$

(iii) In the case of three excitons we find that the ground state wave function originates primarily from the non-Aufbau configuration $h_0^2 h_2^1; e_0^2 e_1^1$. In fact, the third hole prefers to occupy the *p*-like h_2 state rather than the *s*-like h_1 state, due to reduced Coulomb repulsion with the remaining two holes. Two main transitions are possible from the three-exciton ground state: the $e_0 \rightarrow h_0$ recombination, which leaves the system in the excited biexciton configuration $h_0^1 h_2^1; e_0^1 e_1^1$, leads to peak A_3 located at 2.188 eV. The $e_1 \rightarrow h_2$ recombination, which takes the system into the ground state biexciton configuration $h_0^2; e_0^2$, is responsible for peak B_3 centered at 2.497 eV. Note that the B_3 transition originates from an exchange-split triexciton state (see Fig. 8) which is thermally populated; hence the relatively weak oscillator strength of the B_3 transition.

Note that a calculation considering only ground state to ground state transitions would miss most of the peaks observed in Fig. 9. The capability of the CI expansion to access excited states, coupled with the possibility of using a multiband pseudopotential Hamiltonian for the calculation of the single-particle energies and wave functions, makes it the method of choice for calculating excited states of semiconductor quantum dots.

V. CONCLUSION

We have studied the effects of correlation on a simplified, single-band model dot using both QMC and CI, and have studied correlation in the multiexciton PL spectra of a realistically modeled CdSe dot using CI. Our results for the simplified, single-band model are summarized in Table II. We find the following results for our model: (1) total energies for an exciton, a biexciton, and two electrons are dominated by mean-field effects, so that correlation energies and CI convergence errors are less than 1% [see Fig. 3]; (2) typical exciton transition energies, which are ~ 1 eV, can be calculated to closer than 1% by perturbation theory, with only a ~ 2 meV correlation correction [see Fig. 4(a)]; (3) typical exciton binding energies are ~ 46 meV, with only 2 meV from correlation, and our CI captures roughly half of the correlation to give exciton binding energies that are nearly 98% of the exact QMC value; (4) typical biexciton binding energies are positive ~ 6 meV, almost entirely due to correlation energy, and our CI recovers only about 65% of the exact QMC value [see Fig. 4(b)]; (5) exciton charging energies are ~ 1130 meV and well described by CI, while exciton addition energies can be due entirely to correlation, in which case our CI is only qualitatively correct; and (6) typical electron charging energies are ~ 150 meV, of which correlation contributes very little (~ 1 meV); likewise, electron addition energies are ~ 40 meV with very little correlation contribution, so that CI is accurate to about 1–2 % for electron addition energies.

Although QMC is a good method for testing convergence of CI on a simplified, single-band model, only CI may be used on our more realistic model of CdSe. Our multiband pseudopotential model captures the correct symmetries and electronic structure of the dots, leading to qualitatively different predictions from those of single-band models. For example, the multiplet structure presented in Fig. 8 requires a multiband description of the single-particle levels. Some of the details of our realistic CdSe calculation that are missing from our single-band CI model are (1) different degeneracies of the single-particle hole levels due to a multiband description of the valence band states, (2) electron-hole exchange splitting of 5 meV in the ground state (h_0^1, e_0^1) exciton, and (3) the existence of many weak transitions that are symmetry forbidden in single band models. An additional benefit of CI is that it gives excited state energies necessary to identify some of the peaks that appear in single-dot photoluminescence spectra.

We conclude that correlation effects are important to some quantities, such as exciton binding and exciton addition energies, and essential to calculate positive binding energies. QMC methods are well suited for simple, single-band models. Applications to realistic models that capture the proper symmetries and electronic structure of quantum dots are currently restricted to CI methods. We find that CI calculations including all bound states are accurate to better than 3% for many measurable properties, as listed in Table II. Even for biexciton binding, which is dominated by correlation, our CI calculations are qualitatively correct, capturing about 65% of the QMC prediction for a simplified model. Therefore we conclude that a realistic multiband model combined with perturbation theory and a judicious use of CI for correlation corrections is a computational approach well suited to realistic modeling of interacting electrons and holes in SK and colloidal semiconductor quantum dots.

ACKNOWLEDGMENTS

This work was supported by the DOE Office of Science–Basic Energy Sciences, Division of Materials Sciences, Condensed Matter Physics, under Contract No. DE-AC36-99GO10337.

[1] D. Bimberg, M. Grundman, and N. N. Ledentsov, *Quantum Dots Heterostructures* (Wiley, New York, 1999).
[2] U. Woggon, *Optical Properties of Semiconductor Quantum Dots* (Springer-Verlag, Berlin, 1997).
[3] L. Jacak, A. Wójs, and P. Harylack, *Quantum Dots* (Springer-Verlag, Berlin, 1998).
[4] J.-Y. Marzin, J.-M. Gérard, A. Izraël, D. Barrier, and G. Bastard, Phys. Rev. Lett. **73**, 716 (1994).
[5] S. Fafard, R. Leon, D. Leonard, J. L. Merz, and P. M. Petroff, Phys. Rev. B **52**, 5752 (1995).
[6] W. Yang, H. Lee, T. J. Johnson, P. C. Sercell, and A. G. Norman, Phys. Rev. B **61**, 2784 (2000).
[7] E. Dekel, D. Gershoni, E. Ehrenfreund, D. Spektor, J. M. García, and P. M. Petroff, Phys. Rev. Lett. **80**, 4991 (1998).
[8] E. Dekel, D. Gershoni, E. Ehrenfreund, J. García, and P. M. Petroff, Phys. Rev. B **61**, 11 009 (2000).
[9] L. Landin and M.-E. Pistol, C. Pryor, M. Persson, L. Sammuelson, and M. Miller, Phys. Rev. B **60**, 16 640 (1999).
[10] Y. Toda, O. Moriwake, M. Nishioda, and Y. Arakawa, Phys. Rev. Lett. **82**, 4114 (1999).
[11] A. Zrenner, J. Chem. Phys. **112**, 7790 (2000).
[12] M. Fricke, A. Lork, J. P. Kotthaus, G. Medeiros-Ribeiro, and P. M. Petroff, Europhys. Lett. **36**, 197 (1996).
[13] S. Tarucha, D. G. Austing, T. Honda, R. J. van der Hage, and L. P. Kouwenhoven, Phys. Rev. Lett. **77**, 3613 (1996).
[14] U. Banin, Y. Cao, D. Katz, and O. Millo, Nature (London) **400**, 542 (1999).
[15] P. L. McEuen, E. B. Foxman, U. Meiraav, M. A. Kastner, Y. Meir, N. S. Wingreen, and S. J. Wind, Phys. Rev. Lett. **66**, 1926 (1991).

[16] P. L. McEuen, E. B. Foxman, U. Meirav, M. A. Kastner, Y. Meir, N. S. Wingreen, and S. J. Wind, Phys. Rev. B **45**, 11 419 (1992).
[17] M. G. Bawendi, M. Steigerwald, and L. E. Brus, Annu. Rev. Phys. Chem. **41**, 477 (1990).
[18] A. Zrenner, M. Markmann, E. Beham, F. Findeis, G. Böhm, and G. Abstreiter, J. Electron. Mater. **28**, 542 (1999).
[19] K. Brunner, G. Abstreiter, G. Böhm, G. Tränkle, and G. Weimann, Phys. Rev. Lett. **73**, 1138 (1994).
[20] A. Kuther, M. Bayer, A. Forcel, A. Gorbiunov, V. B. Timofeev, F. Schäfer, and J. P. Reithmaier, Phys. Rev. B **58**, R7508 (1998).
[21] H. Kamada, H. Ando, J. Temmyo, and T. Tamamura, Phys. Rev. B **58**, 16 243 (1998).
[22] V. D. Kulakovskii, G. Bacher, R. Weigand, T. Kümmell, A. Forchel, E. Borovitskaya, K. Leonardi, and D. Hommel, Phys. Rev. Lett. **82**, 1780 (1999).
[23] F. Gindele, K. Hild, W. Langbein, and U. Woggon, Phys. Rev. B **60**, R2157 (1999).
[24] R. J. Warburton, B. T. Miller, C. S. Dürr, C. Bödefeld, K. Karrai, J. P. Kotthaus, G. Medeiros-Ribeiro, P. M. Petroff, and S. Haunt, Phys. Rev. B **58**, 16 221 (1998).
[25] A. Barenco and M. A. Dupertuis, Phys. Rev. B **52**, 2766 (1995).
[26] A. Franceschetti, H. Fu, L. W. Wang, and A. Zunger, Phys. Rev. B **60**, 1819 (1999).
[27] A. Franceschetti and A. Zunger, Appl. Phys. Lett. **76**, 1731 (2000).
[28] A. Franceschetti, A. Williamson, and A. Zunger, J. Phys. Chem. B **104**, 3398 (2000).
[29] A. J. Williamson, A. Franceschetti, and A. Zunger, Eur. Phys. Lett. **53**, 59 (2001).
[30] A. Franceschetti and A. Zunger, Phys. Rev. Lett. **78**, 915 (1997).
[31] A. Harju, V. A. Sverdlov, R. M. Nieminen, and V. Halonen, Phys. Rev. B **59**, 5622 (1999).
[32] E. J. Austin, Semicond. Sci. Technol. **3**, 960 (1988).
[33] F. Bolton, Phys. Rev. B **54**, 4780 (1996).
[34] J. Shumway, L. R. C. Fonseca, J. P. Leburton, R. M. Martin, and D. M. Ceperley, Physica E **8**, 260 (2000).
[35] F. Pederiva, C. J. Umrigar, and E. Lipparini, Phys. Rev. B **62**, 8120 (1999).
[36] E. Lee, A. Puzder, My. Y. Chou, T. Uzer, and D. Farrelly, Phys. Rev. B **57**, 12 281 (1998).
[37] F. Luczak, F. Brosens, J. T. Devreese, and L. F. Lemmens, cond-mat/0002343 (unpublished).
[38] C. H. Mak, R. Egger, and H. Weber-Gottschick, Phys. Rev. Lett. **81**, 4533 (1998).
[39] R. Egger, W. Häusler, C. H. Mak, and H. Grabert, Phys. Rev. Lett. **82**, 3320 (1999).
[40] R. Egger, W. Häusler, C. H. Mak, and H. Grabert, Phys. Rev. Lett. **83**, 462 (1999).
[41] R. Egger and C. H. Mak, cond-mat/9910496 (unpublished).
[42] L. Mitas, J. C. Grossman, I. Stich, and J. Tobik, Phys. Rev. Lett. **84**, 1479 (2000).
[43] L.-W. Wang and A. Zunger, J. Phys. Chem. **100**, 2394 (1994).
[44] L.-W. Wang and A. Zunger, J. Phys. Chem. **100**, 2394 (1994).
[45] L. W. Wang and A. Zunger, in *Semiconductor Nanoclusters*, edited by P. V. Kamat and D. Meisel (Elsevier, Amsterdam, 1996).
[46] H. Fu, L.-W. Wang, and A. Zunger, Phys. Rev. B **57**, 9971 (1999).
[47] L.-W. Wang and A. Zunger, J. Phys. Chem. B **102**, 6449 (1998).
[48] L. W. Wang, A. J. Williamson, A. Zunger, H. Jiang, and J. Singh, Appl. Phys. Lett. **76**, 339 (2000).
[49] O. Stier, M. Grundmann, and D. Bimberg, Phys. Rev. B **59**, 5688 (1999).
[50] M. Grundmann, O. Stier, and D. Bimberg, Phys. Rev. B **52**, 11 969 (1995).
[51] D. M. Ceperley and B. Bernu, J. Chem. Phys. **89**, 6316 (1988).
[52] B. Bernu, D. M. Ceperley, and W. A. Lester, Jr., J. Chem. Phys. **93**, 552 (1990).
[53] W. L. McMillian, Phys. Rev. **138**, A442 (1965).
[54] G. Bastard, *Wave Mechanics Applied to Semiconductor Heterostructures* (Les Editions de Physique, Les Ulis Cedex, France, 1988).
[55] D. M. Ceperley and M. H. Kalos, in *Monte Carlo Methods in Condensed Matter Physics*, Vol. 7 of *Topics in Current Physics*, edited by K. Binder (Springer, Heidelberg, 1979), Chap. 4.
[56] K. E. Schmidt and M. H. Kalos, in *Applications of the Monte Carlo Methods in Condensed Matter Physics*, Vol. 36 of *Topics in Current Physics*, edited by K. Binder (Springer, Heidelberg, 1984), Chap. 4.
[57] J. Harting, O. Mülken, and P. Borrmann, cond-mat/0002269 (unpublished).
[58] P. Hawrylak, Phys. Rev. B **60**, 5597 (1999).
[59] P. Hawrylak, G. A. Narvaez, M. Bayer, and A. Forchel, Phys. Rev. Lett. **85**, 389 (2000).
[60] P. Hawrylak, Phys. Status Solidi B **220**, 19 (2000).
[61] M. Braskén, M. Lindberg, D. Sundholm, and J. Olsen, Phys. Rev. B **61**, 7652 (2000).
[62] M. Dib, M. Chamarro, V. Volitos, J. L. Fave, C. Guenaud, P. Roussingnol, T. Gacoin, J. P. Boilot, C. Delerue, G. Allan, and M. Lannoo, Phys. Status Solidi B **212**, 293 (1999).
[63] P. R. C. Kent, M. D. Towler, R. J. Needs, and G. Rajagopal, Phys. Rev. B **62**, 15 394 (2000).
[64] T. Torelli and L. Mitas, Phys. Rev. Lett. **85**, 1702 (2000).
[65] M. Nirmal, D. J. Norris, M. Kuno, M. G. Bawendi, A. L. Efros, and M. Rosen, Phys. Rev. Lett. **75**, 3728 (1995).